

Holography, Heavy-Quark Free Energy, and the QCD Phase Diagram

Pietro Colangelo

Istituto Nazionale di Fisica Nucleare, Sezione di Bari, Italy

Floriana Giannuzzi

*Dipartimento di Fisica, Università degli Studi di Bari
and Istituto Nazionale di Fisica Nucleare, Sezione di Bari, Italy*

Stefano Nicotri

*Institute for Particle Physics Phenomenology, Department of Physics,
Durham University, Durham DH1 3LE, United Kingdom*

We use gauge/string duality to investigate the free energy of two static color sources (a heavy quark-antiquark pair) in a Yang-Mills theory in strongly interacting matter, varying temperature and chemical potential. The dual space geometry is Anti-de Sitter with a charged black-hole to describe finite temperature and density in the boundary theory, and we also include a background warp factor to generate confinement. The resulting deconfinement line in the $\mu - T$ plane is similar to the one obtained by lattice and effective models of QCD.

PACS numbers: 11.25.Tq, 25.75.Nq

Consider QCD in a four dimensional Euclidean space-time and in nuclear matter, and two static color sources, an infinitely heavy quark and an infinitely heavy antiquark, at distance r from each other. It is interesting to investigate how the free energy of such a system behaves against variations of temperature and chemical potential.

The study of a strongly coupled Yang-Mills theory, such as QCD, is a challenge in spite of the methods developed so far to deal with it (lattice simulations, models and effective field theories). The formulation of the gauge/gravity (or Anti-de Sitter/conformal field theory) correspondence [1–4] has suggested to face this problem through the identification of a suitable higher dimensional gravity dual. Due to the strong/weak nature of the duality, the gravity dual is a weakly coupled theory defined in a higher dimensional curved spacetime; since QCD is not conformal, a mechanism for breaking conformal invariance must be included in the dual model.

This holographic framework can be adopted to analyze finite temperature and density effects. In a bottom-up approach, we use the soft wall AdS/QCD model, a five dimensional model formulated on AdS_5 spacetime, in which linear confinement at zero temperature and density is obtained by inserting a background warp factor [5–7], bringing a mass scale related to Λ_{QCD} . To describe the boundary theory at finite temperature, a black-hole is included in the five dimensional space, whose horizon position represents the (inverse) temperature [4].

On the other hand, in QCD the effect of finite quark density is introduced by adding the term $J_D = \mu \psi^\dagger(x) \psi(x)$ to the Lagrangian in the generating functional, so that the chemical potential μ appears as the source of the quark density operator. According to the AdS/CFT correspondence, the source of a QCD operator in the generating functional is the boundary value of a dual field in the bulk; therefore, the chemical potential can be considered as the boundary value of the time com-

ponent of a $U(1)$ gauge field A_M dual to the vector quark current. Under the ansatz $A_0 = A_0(z)$ (z is the fifth holographic coordinate) and $A_i = A_z = 0$ ($i = 1, 2, 3$), one can find a solution of the equations of motion of a $5D$ gravity action with negative cosmological constant interacting with an electromagnetic field: the solution is known as the AdS /Reissner-Nordström black-hole metric, and describes a charged black hole interacting with the electromagnetic field [8, 9]. We use this (Euclidean) metric in our model:

$$ds^2 = \frac{R^2 e^{c^2 z^2}}{z^2} \left(f(z) dt^2 + d\vec{x}^2 + \frac{dz^2}{f(z)} \right),$$

$$f(z) = 1 - \left(\frac{1}{z_h^4} + q^2 z_h^2 \right) z^4 + q^2 z^6, \quad (1)$$

where R is the AdS radius, q the black-hole charge and z_h the position of the horizon, defined by the condition $f(z_h) = 0$. The $e^{c^2 z^2}$ term, characterizing the soft wall model, distorts the metric and brings the mass scale c [6, 10]. The positive sign in the exponent is chosen, following ref.[6], to obtain a confining $\bar{Q}Q$ potential at $T = 0$. The profile introduced in [7], with the negative sign, also produces linear Regge trajectories and bound states for light hadrons, but does not provides an area law for the Wilson loop, as discussed, in the framework of light front holography, in [11]¹. The boundary $z = 0$ represents the four dimensional spacetime on which the Yang-Mills theory is defined.

The Hawking temperature of the black-hole is

$$T = \frac{1}{4\pi} \left| \frac{df}{dz} \right|_{z=z_h} = \frac{1}{\pi z_h} \left(1 - \frac{1}{2} Q^2 \right), \quad (2)$$

¹ Issues related to the choice of the dilaton profile are discussed in [12].

where $Q = qz_h^3$ and $0 \leq Q \leq \sqrt{2}$; moreover, the Euclidean time is a periodic variable, with period $\beta = 1/T$ [4, 13]. Studies of this kind of models for $q = 0$ can be found in [14].

The relation between the parameters in the metric (1) and the chemical potential can be obtained observing that, on dimensional grounds, the low z behavior of the bulk gauge field $A_0(z)$ is

$$A_0(z) = \mu - \eta z^2 \quad (3)$$

with $\eta = \kappa q$ and κ a dimensionless parameter in our model. Together with the condition that A_0 vanishes at the horizon, $A_0(z_h) = 0$, Eq.(3) determines a relation between μ and the black-hole charge:

$$\mu = \kappa q z_h^2 = \kappa \frac{Q}{z_h}. \quad (4)$$

The parameter c in the warp factor in (1) sets the scale: in the following, we analyze quantities expressed in units of c , and comment on the numerical results at the end.

Let us now turn to the problem formulated at the beginning of this study. At finite temperature, the free energy $F(r, T)$ of an infinitely heavy quark-antiquark pair at distance r can be obtained in QCD from the correlation function of two Polyakov loops:

$$\langle \mathcal{P}(\vec{x}_1) \mathcal{P}^\dagger(\vec{x}_2) \rangle = e^{-\frac{1}{T} F(r, T) + \gamma(T)} \quad (5)$$

with $r = |\vec{x}_1 - \vec{x}_2|$ and $\gamma(T)$ a normalization constant. Moreover, the expectation value of a single Polyakov loop

$$\langle \mathcal{P} \rangle = e^{-\frac{1}{2T} F^\infty(T)} \quad (6)$$

($F^\infty(T) = F(r = \infty, T)$ and neglecting the normalization) is the order parameter for the deconfinement transition in a pure $SU(N)$ theory [15]. Within the gauge/string duality approach, we can attempt a calculation of the expectation values in (5) and (6) considering string configurations in the 5D manifold having the Polyakov loops as boundary, looking at the configurations of minimal surfaces and computing their worldsheet action. The worldsheet action is the Nambu-Goto one

$$S_{\text{NG}} = \frac{1}{2\pi\alpha'} \int d^2\xi \sqrt{\det [g_{MN} (\partial_a X^M) (\partial_b X^N)]} \quad (7)$$

for a string with endpoints attached to the positions of the heavy quark and antiquark, $x = \pm r/2$ at $z = 0$, so that [16, 17]

$$F(r, T) = T S_{\text{NG}}. \quad (8)$$

X^M 's are the coordinates of the five dimensional space-time, g_{MN} the metric tensor associated to the line element (1), and the determinant is taken over the indices $a, b = 0, 1$ labeling the worldsheet coordinates ξ^a . We parametrize them with $\xi^0 = t$ and $\xi^1 = x$, and look for a static solution $z(x)$ satisfying the conditions $z(x=0) = z_0$, $z'(x=0) = 0$ and $z(x = \pm r/2) = 0$, the

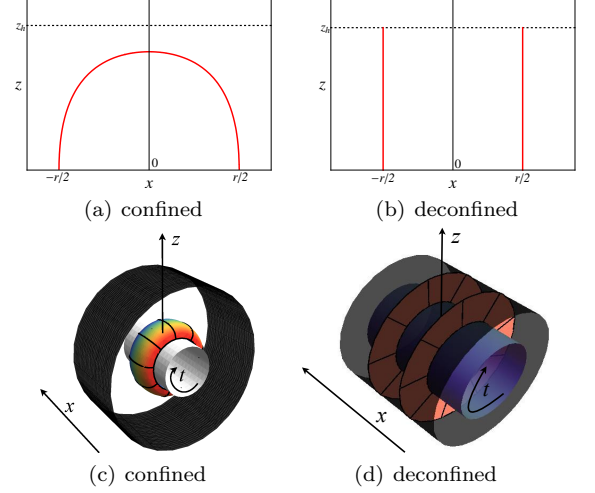


Figure 1: String configurations corresponding to the confined (a,c) and deconfined phase (b,d). In (a,c) there is one string with endpoints at the positions of the static color sources, $x = \pm r/2$ at $z = 0$, which does not intersect the horizon (dark cylinder in (c)); in (b,d) there are two strings stretched between $z = 0$ and the horizon $z = z_h$, with $x(z) = \pm r/2$.

prime denoting the derivative with respect to x . Examples of such configurations are shown in Fig. 1(a)-1(d).

From (7) and (8) we obtain an expression for the free energy:

$$F(r, T) = \frac{g}{\pi} \int_{-r/2}^0 dx \frac{e^{c^2 z^2}}{z^2} \sqrt{f(z) + (z')^2} \quad (9)$$

with $g = \frac{R^2}{\alpha'}$. Moreover, an equation of motion follows from (9), with the first integral

$$\mathcal{H} = \frac{e^{c^2 z^2}}{z^2} \frac{f(z)}{\sqrt{f(z) + (z')^2}} \quad (10)$$

which allows us to express $F(r, T)$ in terms of z_0 and $f_0 = f(z_0)$. Defining $v = z/z_0$, after having subtracted the UV ($v \rightarrow 0$) divergence (corresponding to subtract the infinite quark and antiquark mass in four dimensional QCD[16]), we obtain

$$\hat{F}(\lambda) = \frac{g}{\pi\lambda} \left[-1 + \int_0^1 \frac{dv}{v^2} \left(\frac{e^{\lambda^2 v^2}}{\tau(v)} - 1 \right) \right] \quad (11)$$

where $\hat{F} = F/c$, $\lambda = c z_0$ and

$$\tau(v) = \sqrt{1 - \frac{f_0}{f(z_0 v)} v^4 e^{2\lambda^2(1-v^2)}}. \quad (12)$$

The distance $\hat{r} = cr$ can also be expressed parametrically,

$$\hat{r}(\lambda) = 2\lambda\sqrt{f_0} \int_0^1 dv \frac{v^2 e^{\lambda^2(1-v^2)}}{\tau(v)f(z_0 v)}, \quad (13)$$

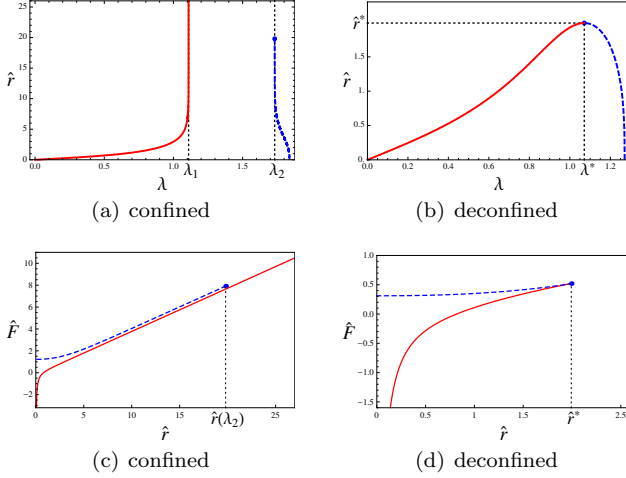


Figure 2: Interquark distance $\hat{r}(\lambda)$ in the confined (a) and deconfined phase (b). In (a) (here for $\hat{\mu} = 0.5$ and $\hat{T} = 0.82T^*$), for $0 \leq \lambda \leq \lambda_1$, $\hat{r}(\lambda)$ spans the whole real axis (red solid line); as $\lambda_2 \leq \lambda \leq \hat{z}_h$, $\hat{r}(\lambda)$ monotonically decreases from a finite value $\hat{r}(\lambda_2)$ to $\hat{r}(\hat{z}_h) = 0$ (blue dashed line). The free energies corresponding to the two branches are plotted in (c). In (b) (here for $\hat{\mu} = 0.5$ and $\hat{T} = 1.65T^*$) $\hat{r}(\lambda)$ has a maximum for $\lambda_1 = \lambda_2 = \lambda^*$; the free energy is plotted in (d).

so that, from (11) and (13) we can write the free energy as a function of the temperature $\hat{T} = T/c$, for a range of values of the chemical potential $\hat{\mu} = \mu/c$. We fix the parameters κ and g to one, postponing to the end the discussion on the numerical results.

As for $\hat{\mu} = 0$ [17], also for finite chemical potential the distance $\hat{r}(\lambda)$, written parametrically in (13), has two branches, shown in Fig. 2(a). For $0 \leq \lambda \leq \lambda_1$, \hat{r} increases monotonically from $\hat{r}(0) = 0$, spans the whole real axis and diverges when $\lambda \rightarrow \lambda_1$. For $\lambda_2 \leq \lambda \leq \hat{z}_h = cz_h$, \hat{r} monotonically decreases from a finite value $\hat{r}(\lambda_2)$ down to $\hat{r}(\hat{z}_h) = 0$; for $\lambda_1 < \lambda < \lambda_2$, \hat{r} has an imaginary part. Selecting the branch $0 \leq \lambda \leq \lambda_1$, we can compute \hat{F} for all distances, with the result depicted in Fig. 2(c). As shown in the same figure, the values of the free energy corresponding to the branch $\lambda_2 \leq \lambda \leq \hat{z}_h$ are larger than those for $0 \leq \lambda \leq \lambda_1$. The resulting free energy can be parameterized similarly to the Cornell expression for the static quark-antiquark potential:

$$\hat{F} = -\frac{a}{\hat{r}} + \hat{b} + \hat{\sigma}^2 \hat{r} . \quad (14)$$

The coefficient a turns out to be essentially independent of T and μ ; on the other hand, at fixed $\hat{T} = 0.05$, the parameter \hat{b} increases, from $\hat{b} = -0.073$ at $\hat{\mu} = 0$ to $\hat{b} = -0.051$ at $\hat{\mu} = 0.6$, while $\hat{\sigma}$ decreases from $\hat{\sigma} = 0.64$ to $\hat{\sigma} = 0.62$ when $\hat{\mu}$ is changed from $\hat{\mu} = 0$ to $\hat{\mu} = 0.6$.

For fixed values of the chemical potential $\hat{\mu} = \hat{\mu}^*$, increasing \hat{T} , the two points λ_1 and λ_2 along the λ axis get closer to each other, and at a certain value \hat{T}^* they coincide: $\lambda_1 = \lambda_2 = \lambda^*$. For $\hat{T} \geq \hat{T}^*$, $\hat{r}(\lambda)$ is real for

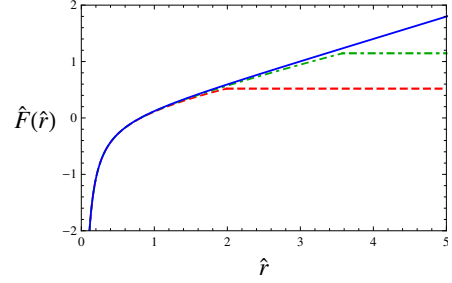


Figure 3: Free energy in the confined phase, $\hat{\mu} = 0.5$, $\hat{T} = 0.82T^*$ (blue solid line), and in the deconfined one, for $\hat{\mu} = 0.5$, $\hat{T} = 1.23T^*$ (green dot-dashed) and $\hat{\mu} = 0.5$, $\hat{T} = 1.65T^*$ (red dashed). For $\hat{\mu} = 0.5$ the critical temperature is $\hat{T}^* = 0.122$.

$0 \leq \lambda \leq \hat{z}_h$, and never exceeds the value $\hat{r}(\lambda^*)$, as shown in Fig. 2(b): at the point $(\hat{\mu}^*, \hat{T}^*)$ in the $\hat{\mu} - \hat{T}$ plane $\hat{r}(\lambda)$ is always bounded. Therefore, taking $\hat{\mu} = \hat{\mu}^*$ and $\hat{T} \geq \hat{T}^*$, \hat{F} can be evaluated only for $\hat{r} \leq \hat{r}(\lambda^*)$, Fig. 2(d). For $\hat{r} > \hat{r}(\lambda^*)$ there is another string configuration, *i.e.* the one with two strings stretched between the boundary $\hat{z} = 0$ and the black-hole horizon $\hat{z} = \hat{z}_h$, plotted in Figs. 1(b) and 1(d) [18]. This configuration holographically represents two deconfined quarks. To evaluate the corresponding action we choose a different parametrization of the worldsheet: $\xi^0 = t$ and $\xi^1 = z$, obtaining the regularized free energy

$$\hat{F}^\infty = \frac{g}{\pi} \left[-\frac{1}{\hat{z}_h} + \int_0^{\hat{z}_h} \frac{d\hat{z}}{\hat{z}^2} \left(e^{\hat{z}^2} - 1 \right) \right] + \zeta(\hat{\mu}, \hat{T}) \quad (15)$$

with $\hat{z} = cz$; $\zeta(\hat{\mu}, \hat{T})$ is a constant related to the regularization procedure, and fixed by matching $\hat{F}(\hat{r}^*) = \hat{F}^\infty$. In this case the free energy does not depend on \hat{r} , but only on the temperature and chemical potential.

As a result, the free energy is depicted in Fig. 3. At large values of \hat{r} , for a given value of the chemical potential $\hat{\mu}$ there is a temperature $\hat{T}^*(\hat{\mu})$ such that for \hat{T} less than \hat{T}^* the free energy linearly grows with \hat{r} , while for $\hat{T} \geq \hat{T}^*$ the solution coming from the connected string configuration (Fig. 1(a)) is only valid up to $\hat{r} = \hat{r}(\lambda^*)$; from that point on, \hat{F} is constant (15). This behavior of the free energy with distance and temperature has been observed in quenched lattice simulations at $\hat{\mu} = 0$ [19].

In the $\hat{\mu} - \hat{T}$ plane, the curve defined by the points $(\hat{\mu}, \hat{T}^*(\hat{\mu}))$ is plotted in Fig. 4. This can be considered as a picture of the deconfinement transition in the QCD phase diagram. For low values of T and μ there is a confined phase characterized by a linearly increasing interquark potential. Outside this region, a finite amount of energy is sufficient to separate the quark-antiquark pair, as expected in a deconfined phase. The picture agrees with the diagram obtained by, *e.g.*, Nambu-Jona-Lasinio [20] and other effective models [21].

In the same holographic framework, the Polyakov loop $\langle P \rangle$ can be computed by Eq.(6). In the confined phase,

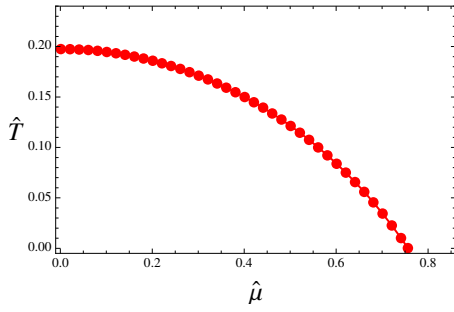


Figure 4: Deconfinement transition line in the $\hat{\mu} - \hat{T}$ plane. The line divides the plane in two regions, a hadron phase near the origin, and a deconfined phase beyond the curve.

$\hat{F}(\hat{r})$ diverges as $\hat{r} \rightarrow \infty$, so $\langle \mathcal{P} \rangle$ vanishes, while in the deconfined one it is determined by \hat{F}^∞ from the configuration in Figs. 1(b) and 1(d). The result is depicted in Fig. 5: for each value of $\hat{\mu}$, the Polyakov loop vanishes as $\hat{T} < \hat{T}^*$; it starts growing at $\hat{T} = \hat{T}^*$ [22]. The smooth increase can be interpreted as a continuous transition between the hadron and the deconfined phase.

As pointed out in [9], the parameter κ scales as $\kappa \sim \sqrt{N_c}$ and its numerical value is model dependent. If we take the limit $N_c \rightarrow \infty$, the deconfinement line in Fig. 4 becomes flat, with \hat{T}^* not depending on $\hat{\mu}$, in agreement with the result found in [23]. Considering a finite κ in (4), the deconfinement line has the shape shown in Fig. 4.

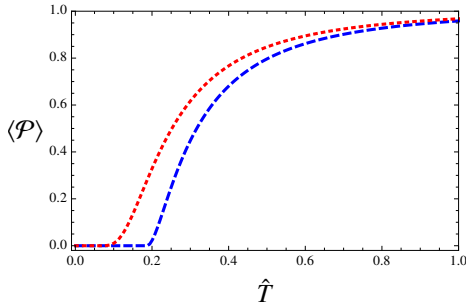


Figure 5: Polyakov loop $\langle \mathcal{P} \rangle$ versus \hat{T} (normalized at its value for $T \rightarrow \infty$) for $\hat{\mu} = 0.2$ (blue, dashed, right curve) and $\hat{\mu} = 0.7$ (red, dotted, left curve).

In order to discuss numerical results, we need to choose the values of the parameter κ in (4) and of the mass scale c appearing in the warp factor. We fix $\kappa \approx 1/2$ from the ratio $\hat{T}_c/\hat{\mu}_c \approx 0.5$ found in [20], with $\hat{T}_c = \hat{T}^*$ at $\hat{\mu} = 0$ and $\hat{\mu}_c = \hat{\mu}^*$ at $\hat{T} = 0$ (κ could also be determined in this soft wall model studying different observables, as done in [9] for the hard wall model). The mass scale c induced by the warp factor can be fixed from the result $T_c \approx 170$ MeV [24]: $c \approx 850$ MeV. On the other hand, the value of this scale from the ρ meson mass is $c \approx 670$ MeV [5], which gives $T_c \approx 134$ MeV and $\mu_c \approx 248$ MeV.²

The numerical values of the critical chemical potential are a remarkable result of our study. The other result is that the gauge/string duality approach can be used to obtain information on the deconfinement transition in QCD, finding an agreement with the outcome of effective theories (even if the model is not sensitive to the structure of the vacuum). The success of the holographic framework is noticeable, considering the difficulty of lattice QCD to explore the phase diagram along the axis of the chemical potential, and opens interesting perspectives for the analysis, for example, of the superconducting phases of QCD.

Acknowledgments

We are grateful to Fulvia De Fazio and Marco Ruggieri for discussions. This work was supported, in part, by the EU contract No. MRTN-CT-2006-035482, “FLAVIANet”. FG was supported, in part, by the grant “*Borse di ricerca in collaborazione internazionale*” by *Regione Puglia, Italy*; she thanks the IPPP, Durham, for hospitality during the completion of this work.

-
- [1] J. M. Maldacena, Adv. Theor. Math. Phys. **2**, 231 (1998).
 - [2] E. Witten, Adv. Theor. Math. Phys. **2**, 253 (1998).
 - [3] S. S. Gubser, I. R. Klebanov and A. M. Polyakov, Phys. Lett. B **428**, 105 (1998).
 - [4] E. Witten, Adv. Theor. Math. Phys. **2**, 505 (1998).
 - [5] O. Andreev, Phys. Rev. D **73**, 107901 (2006).
 - [6] O. Andreev and V. I. Zakharov, Phys. Rev. D **74**, 025023 (2006).
 - [7] A. Karch, E. Katz, D. T. Son and M. A. Stephanov, Phys. Rev. D **74**, 015005 (2006).
 - [8] A. Chamblin, R. Emparan, C. V. Johnson and R. C. Myers, Phys. Rev. D **60**, 064018 (1999), Phys. Rev. D **60**, 104026 (1999).
 - [9] B. H. Lee, C. Park and S. J. Sin, JHEP **0907**, 087 (2009); K. Jo, B. H. Lee, C. Park and S. J. Sin, JHEP **1006**, 022 (2010).
 - [10] O. Andreev, Phys. Rev. D **81**, 087901 (2010).
 - [11] G. F. de Teramond and S. J. Brodsky, Nucl. Phys. Proc. Suppl. **199**, 89 (2010).
 - [12] A. Karch, E. Katz, D. T. Son and M. A. Stephanov, arXiv:1012.4813 [hep-ph].
 - [13] C. P. Herzog, Phys. Rev. Lett. **98**, 091601 (2007).
 - [14] M. Fujita, K. Fukushima, T. Misumi and M. Murata, Phys. Rev. D **80**, 035001 (2009); P. Colangelo, F. Gian-

- nuzzi and S. Nicotri, Phys. Rev. D **80**, 094019 (2009); A. S. Miranda *et al.*, JHEP **0911**, 119 (2009); M. Fujita *et al.*, Phys. Rev. D **81**, 065024 (2010); H. R. Grigoryan, P. M. Hohler and M. A. Stephanov, Phys. Rev. D **82**, 026005 (2010).
- [15] A. M. Polyakov, Phys. Lett. B **72**, 477 (1978); G. 't Hooft, Nucl. Phys. B **138**, 1 (1978).
- [16] J. M. Maldacena, Phys. Rev. Lett. **80**, 4859 (1998); S. J. Rey and J. T. Yee, Eur. Phys. J. C **22**, 379 (2001).
- [17] O. Andreev and V. I. Zakharov, JHEP **0704**, 100 (2007); M. Mia, K. Dasgupta, C. Gale and S. Jeon, arXiv:1006.0055 [hep-th].
- [18] S. J. Rey, S. Theisen and J. T. Yee, Nucl. Phys. B **527**, 171 (1998); A. Brandhuber, N. Itzhaki, J. Sonnenschein and S. Yankielowicz, Phys. Lett. B **434**, 36 (1998).
- [19] O. Kaczmarek, F. Karsch, P. Petreczky and F. Zantow, Phys. Lett. B **543**, 41 (2002).
- [20] M. Buballa, Phys. Rept. **407**, 205 (2005).
- [21] B. J. Schaefer and J. Wambach, Nucl. Phys. A **757**, 479 (2005).
- [22] O. Andreev, Phys. Rev. Lett. **102**, 212001 (2009).
- [23] L. McLerran and R. D. Pisarski, Nucl. Phys. A **796**, 83 (2007).
- [24] Y. Aoki *et al.*, JHEP **0906**, 088 (2009).